Journal of Medicinal Chemistry
Article

J. Med. Chem. **2010,** *53,* 419–431 **419**
DOI: 10.1021/jm901351f

Synthesis, Biological Evaluation, X-ray Structure, and Pharmacokinetics of Aminopyrimidine c-jun-N-terminal Kinase (JNK) Inhibitors

Ted Kamenecka, Rong Jiang, Xinyi Song, Derek Duckett, Weimin Chen, Yuan Yuan Ling, Jeff Habel, John D. Laughlin, Jeremy Chambers, Mariana Figuera-Losada, Michael D. Cameron, Li Lin, Claudia H. Ruiz, and Philip V. LoGrasso*

Department of Molecular Therapeutics, and Translational Research Institute, The Scripps Research Institute, Scripps Florida, 130 Scripps Way A2A, Jupiter, Florida 33458

Received September 14, 2009

Given the significant body of data supporting an essential role for c-jun-N-terminal kinase (JNK) in neurodegenerative disorders, we set out to develop highly selective JNK inhibitors with good cell potency and good brain penetration properties. The structure−activity relationships (SAR) around a series of aminopyrimidines were evaluated utilizing biochemical and cell-based assays to measure JNK inhibition and brain penetration in mice. Microsomal stability in three species, P450 inhibition, inhibition of generation of reactive oxygen species (ROS), and pharmacokinetics in rats were also measured. Compounds **9g**, **9i**, **9j**, and **9l** had greater than 135-fold selectivity over p38, and cell-based IC_{50} values < 100 nM. Moreover, compound **9l** showed an IC_{50} = 0.8 nM for inhibition of ROS and had good pharmacokinetic properties in rats along with a brain-to-plasma ratio of 0.75. These results suggest that biaryl substituted aminopyrimidines represented by compound **9l** may serve as the first small molecule inhibitors to test efficacy of JNK inhibitors in neurodegenerative disorders.

Introduction

Compelling evidence has surfaced over the past eight years supporting JNK as a good therapeutic target for the treatment of neurodegenerative disease. Indeed, numerous reports utilizing either knockout mice or a peptide derived from the JNK-interacting protein (JIP[a]) have shown that loss of JNK activity is protective in animal models of neurodegeneration. For example, in 2001, Xia et al. showed that stereotactic adenoviral transfer of residues 127−281 from JIP into the striatum prevented loss of dopaminergic neurons in the substantia nigra pars compacta (SNpc) and also increased levels of striatal dopamine in mice subchronically treated with 1-methyl-4-phenyl-1,2,3,6-tetrahydropyridine (MPTP).[1] Three years later, Flavell and colleagues showed that *Jnk2*, *Jnk3*, and especially *Jnk2/3* knockout mice were resistant to acute MPTP intoxication where these mice showed significantly less loss of dopaminergic neurons in the SNpc and also increased levels of striatal dopamine compared to wild type mice treated with MPTP.[2] In a similar fashion, Borsello et al. showed that a 20 amino acid JIP peptide fused to the 10-amino acid HIV Tat transporter system delivered by intraventricular injection to adult mice subjected to transient middle cerebral artery occlusion (MCAO) reduced lesion volume by 90% for at least 14 days and prevented behavioral consequences compared to untreated mice.[3] This profound protection correlated with a decrease in c-jun phosphorylation and illustrated the benefit of JNK inhibition as a potential neuroprotective agent for stroke. Like the PD model, *Jnk3* knockout mice also showed protection against cerebral hypoxic ischemia injury in mice. *Jnk3* knockout mice showed only 28% neuronal tissue loss compared to 48% for wild type mice subjected to unilateral hypoxic-ischemia injury.[4] Interestingly, JNK3 is almost exclusively expressed in the brain, with only low level expression seen in the heart and testis,[5] suggesting a potential unique role for this isoform in central nervous system (CNS) disorders. Moreover, numerous reports have implicated JNK as a key regulator of oxidative stress and neuronal death as a result of reactive oxygen species generated in cell models of PD utilizing 6-hydroxy dopamine or MPTP/MPP^+.[6−9] Combined, all of these data are good validation for JNK as a target in CNS disease.

From a chemistry perspective, numerous JNK selective inhibitors have begun to emerge and include compounds from classes such as indazoles,[10,11] aminopyrazoles,[11] aminopyridines,[12,13] pyridine carboxamides,[13,14] benzothien-2-yl-amides and benzothiazol-2-yl acetonitriles,[15,16] quinoline derivatives,[17] and aminopyrimidines.[18,19] For a recent review of all these classes, see LoGrasso and Kamenecka.[20] All of these compounds classes, with the exception of the indazoles, have shown selectivity for JNK over p38, but few have demonstrated good brain penetration, a feature essential for CNS therapeutics. The well-described clinical toxicity of p38 inhibition necessitates this selectivity in any JNK inhibitor program.[21] The only compound class mentioned above to show brain penetration was the benzothiazol-2-yl acetonitrile, represented by AS601245, which was shown to be efficacious

*To whom correspondence should be addressed. Phone: 561-228-2230. Fax: 561-228-3081. E-mail: lograsso@scripps.edu.

[a] Abbreviations: ATP, adenosine triphosphate; AMP-PCP, β,γ-methyleneadenosine 5′-triphosphate; CDK2, cyclin-dependent kinase 2; CM-H_2DCFDA, 5-(and-6)-chloromethyl-2′,7′-dichlorofluorescin diacetate, acetyl ester; CNS, central nervous system; IL-2, inteleukine-2; INS-1, insulinoma-1; JIP, JNK-interacting protein; JNK, c-jun-N-terminal kinase; MCAO, middle cerebral artery occlusion; MPTP, 1-methyl-4-phenyl-1,2,3,6-tetrahydropyridine; PSA, polar surface area; PD, Parkinson's disease; ROS, reactive oxygen species; SNpc, substantia nigra pars compacta, STZ, streptozotocin.

Published on Web 11/30/2009

Scheme 1. General Procedure for the Synthesis of Boronic Esters[a]

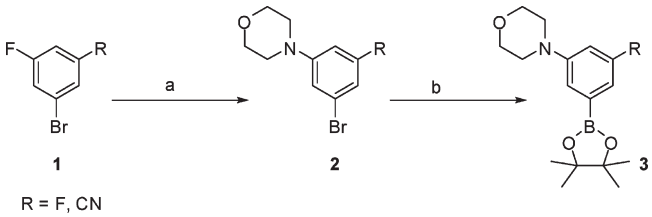

[a] Reagents and conditions: (a) morpholine, 120 °C; (b) Pd(dppf)Cl_2-(CH_2Cl_2), KOAc, bis(pinacolato)diboron, (OR′ = pinacol), DMSO.

in transient global ischemia models in gerbils, albeit at ip doses ≥60 mg/kg.[22,23] More recently, aminopyrimidines similar in structure to those presented in our current work have been reported for peripheral applications such as inflammatory disorders[18] and type II diabetes mellitus.[19] In the study by Alam et al., the key selectivity struggle was versus cyclin-dependent-kinase-2 (CDK2), where phenyl-substituted pyrazolopyridines were single digit nanomolar JNK2 and JNK3 inhibitors showing no inhibition of CDK2 up to 10 μM.[18] Thus, while these compounds are selective versus p38 and potent JNK inhibitors, it is unclear if they are suitable for CNS penetration, as they were not designed with these parameters in the desired compound profile.

The current study was designed to develop JNK3 inhibitors which were selective over p38, had cell-based potency for inhibition of phosphorylation of c-jun near 100 nM, showed functional protection versus oxidative stress, had good pharmacokinetic properties, and had a brain:plasma ration greater than 0.5. These goals were achieved by biaryl substitution of an aminopyrimidine core. Structural features which were especially important for maintaining cellular potency and achieving brain penetration were substitutions which included 1,2,4-morpholino substituted triazoles as represented by compound **9l**. The X-ray crystal structure of **9l** revealed this class of inhibitors to bind in the ATP pocket of JNK3.

Results

Synthesis of Aminopyrimidine JNK Inhibitors. Disubstituted boronate esters (**3**) were prepared as described in Scheme 1. Commercially available aryl fluorides (**1**) were heated in neat morpholine to provide clean SNAr-substitution products (2). Quenching these reactions with water typically resulted in precipitation of product in analytically pure form. Conversion of the aryl bromides to boronate esters was done under standard literature conditions as shown in Scheme 1. Other boronic acids used were commercially available from a variety of vendors.

Aniline synthesis was equally straightforward and is described in Scheme 2. Treatment of 4-fluoro-1-nitrobenzene (**4**) with substituted triazoles resulted in clean conversion to substitution products (**5**). Reduction of the nitro group to amino was typically accomplished via hydrogenation in the presence of a suitable palladium catalyst to provide anilines (**6**). Where R = Br, nitro reduction was carried out by tin-mediated reduction, without loss of the bromine atom. The bromine atom then served as a functional group handle with which to introduce additional groups (both aromatics and amines) later in the synthesis as described in the Experimental Section.

Synthesis of final compounds as described in Table 1 is described in Scheme 3. Suzuki coupling of 2,4-dichloropyrimidine with synthesized boronate esters or commercially

Scheme 2. General Procedure for the Synthesis of Anilines[a]

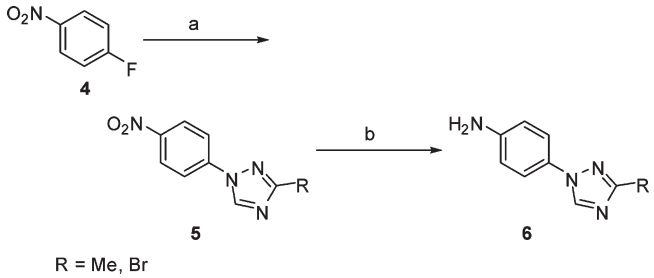

[a] Reagents and conditions: (a) substituted triazole, K_2CO_3, DMF; (b) H_2 or $SnCl_2$.

available boronic acids proceeded uneventfully to provide biaryl intermediates (**8**). In many instances, the crude products after aqueous workup were clean enough to proceed to the final step in the synthesis; however, analytical samples were purified by silica gel chromatography to obtain the appropriate spectral data. Coupling of the 2-chloropyrimidine products with 4-substituted anilines proceeded under two different reaction conditions. The reactants could either be heated in aqueous ethoxyethanol at 120 °C overnight or in anhydrous ethoxyethanol at 190 °C for 1 h. Products were typically precipitated out of the reaction mixture by addition of excess water and were sufficiently pure for in vitro testing or could be purified by silica gel chromatography or reverse-phase preparative HPLC.

Structure−Activity Relationships Affecting Biochemical and Cell-Based Potency for Aminopyrimidines. Table 1 highlights the structures for 12 compounds and presents the biochemical IC_{50} values against JNK1, JNK3, and p38, along with the cell-based IC_{50} for inhibition of c-jun phosphorylation in INS-1 cells treated with streptozotocin (STZ). These 12 compounds were selected from among 500 aminopyrimidines synthesized in our program. All of the compounds had biochemical IC_{50} values < 500 nM versus JNK3. In addition, all 12 compounds had IC_{50} > 20 μM versus p38. Substitution of the amide at R4 (compound **9a**) with a 1,2,4-triazole (compound **9b**) showed no change in the biochemical IC_{50} versus JNK3 (Table 1). The two most potent compounds, **9d** and **9e**, had IC_{50} values = 7 and 4 nM, respectively. Key structure−activity relationship (SAR) elements driving the in vitro potency of compounds **9d** and **9e** were the addition of methyl sulfonamide at the R2 position. Replacement of the sulfonamide moiety in the R4 position of compound **9d** by a 1,2,3-triazole as seen in **9e** had no effect on JNK3 or JNK1 inhibition (Table 1). Converting the 1,2,3-triazole at the R4 position of **9c** to a 3-methyl-1,2,4-triazole (**9f**) had no effect on JNK 3 and JNK1 biochemical inhibition, nor did it affect cell-based inhibition of c-jun phosphorylation (Table 1). When a nitrile group was added to the R3 position (**9g**), an approximate 5-fold increase in potency for JNK3 and JNK1 inhibition was seen compared to **9f** and an approximate 3-fold improved potency was translated to the cell-based readout; inhibition of c-jun phosphorylation (Table 1). When a 2-methyl-1,2,3,4,-tetrazole (**9h**) replaced the 3-methyl-1,2,4-triazole (**9g**), a less than 2-fold difference in IC_{50}s was seen for JNK3, JNK1, and c-jun phosphorylation (Table 1). Finally, 3-pyridyl (**9i** and **9j**) or 3-morpholino (**9l**) substitutions to the 1,2,4-triazole at position R4 had cell-based IC_{50}s approximately 5-fold more potent than *N*-methyl piperazine substituted at that position (**9k**).

Table 1. Biochemical IC_{50}s for Inhibition of JNK1, JNK3, p38, and Cell-Based Inhibition of c-jun for Aminopyrimidines[a]

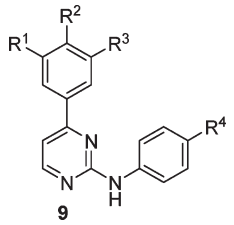

9

Entries	R^1	R^2	R^3	R^4	JNK1 IC_{50} (μM)	JNK3 IC_{50} (μM)	p38 IC_{50} (μM)	c-jun IC_{50} (μM)
9a	H	H	H	$CONH_2$	0.535	0.491	>20	N/A
9b	H	H	H		N/A	0.297	N/A	N/A
9c		H	H		0.123	0.365	>20	0.350
9d	H	$NHSO_2CH_3$	H	SO_2NH_2	0.019	0.007	>20	N/A
9e	H	$NHSO_2CH_3$	H		0.016	0.004	>20	0.210
9f		H	H		0.113	0.390	>20	0.281
9g		H	CN		0.054	0.079	>20	0.089
9h		H	CN		0.045	0.140	>20	0.140
9i		H	H		0.097	0.085	>20	0.083
9j		H	CN		0.039	0.079	>20	0.082
9k		H	F		0.102	0.133	>20	0.260
9l		H	F		0.099	0.148	>20	0.054

[a] The biochemical IC_{50} values are the averages of three or more experiments. The cell-based IC_{50} values are the averages of two or more experiments. All standard deviations ≤39%.

Scheme 3. General Procedure for the Synthesis of Substituted Pyrimidines[a]

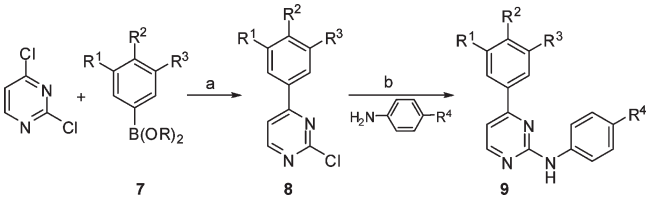

7 **8** **9**

[a] Reagents and conditions: (a) $Pd(PPh_3)_4$, 2 M K_2CO_3 and DME, 90 °C, 10 h, (OR = pinacol or OH); (b) 4-substituted aniline and 2-ethoxyethanol, 120 °C, 10 h.

Crystallography of JNK3-Compound 9l Complex. Utilizing steady state kinetics we had previously shown compound **9a** to be an ATP competitive inhibitor of JNK3,[24] and preliminary unpublished crystallography data from our lab at the time indicated compound **9a** bound in the ATP pocket (unpublished results). In this work, the structure of **9l**-soaked JNK3 crystals were solved at 2.4 Å and refined to final R_{work}/R_{free} of 22.0/26.9 with further refinement statistics presented in Table 2. Figure 1a presents the crystal structure of JNK3 with **9l** bound in the ATP pocket and highlights eight key amino acid residue side chains previously shown to have essential binding contributions for JNK inhibitors.[11,12,25,26] The aminopyrimidine portion of **9l** overlaid nicely with the adenosine portion of AMP-PCP (rmsd = 0.51 Å), and the morpholino group at R1 was found to overlay with the ribose of AMP-PCP as well. A striking feature about this structure was that **9l** did not appear to have any hydrogen bond interactions with any residues in JNK3 due to the relative lack of potential donor and acceptor groups on the ligand. In addition, the highly planar nature of **9l** fit nicely into a groove largely composed of hydrophobic residues but did not cause movement of the Met146 side chain to the back of the ATP binding pocket as seen for other JNK inhibitors.[12,26] A final feature of this structure was that the Gly-rich loop appeared to drop by ~2.5 Å, forming a more compressed active site compared to Merck compound 1 (PDB ID 1PMN) from Scapin et al.[26] The rmsd for this region of the protein was 1.95 Å compared to 1.39 Å for the entire protein. To further illustrate this difference, Figure 1b presents the backbone trace of JNK3 (gray) complexed with compound **9l** overlaid with the backbone of JNK3 (green) from Scapin et al.[26] The glycine-rich loop containing residues I70−V78 was collapsed inward by ~2.5 Å compared to the glycine-rich loop (green) of JNK 3 from 1PMN.[26] The space filling model presented in Figure 1c further illustrates the planar nature of compound **9l** and the hydrophobic interactions which dominate compound **9l** binding to JNK3.

Table 2. X-ray Crystallography Data Collection and Refinement Statistics

data collection		model refinement	
space group	$C222_1$	resolution range (Å)	24−2.4
resolution range (Å)	68−2.4	R_{work}[b] (%)	22.0
no. of unique reflections	13329	R_{free}[b] (%)	26.9
completeness (%)	98.6(87.5)	rmsd bonds (Å)	0.021
R_{sym}[a] (%)	6.2	rmsd angles (deg)	2.107
I/σ	44.7 (2.4)	mean B value (Å^2)	31.973

[a] $R_{sym} = \sum_{hkl}(|(I_i - I)|)/\sum(I)$. [b] $R = \sum(||F_o| - |F_c||)/\sum(|F_o|)$ where R_{free} represents a 5% subset of reflections excluded from refinement. Values in parentheses represent the highest resolution shell.

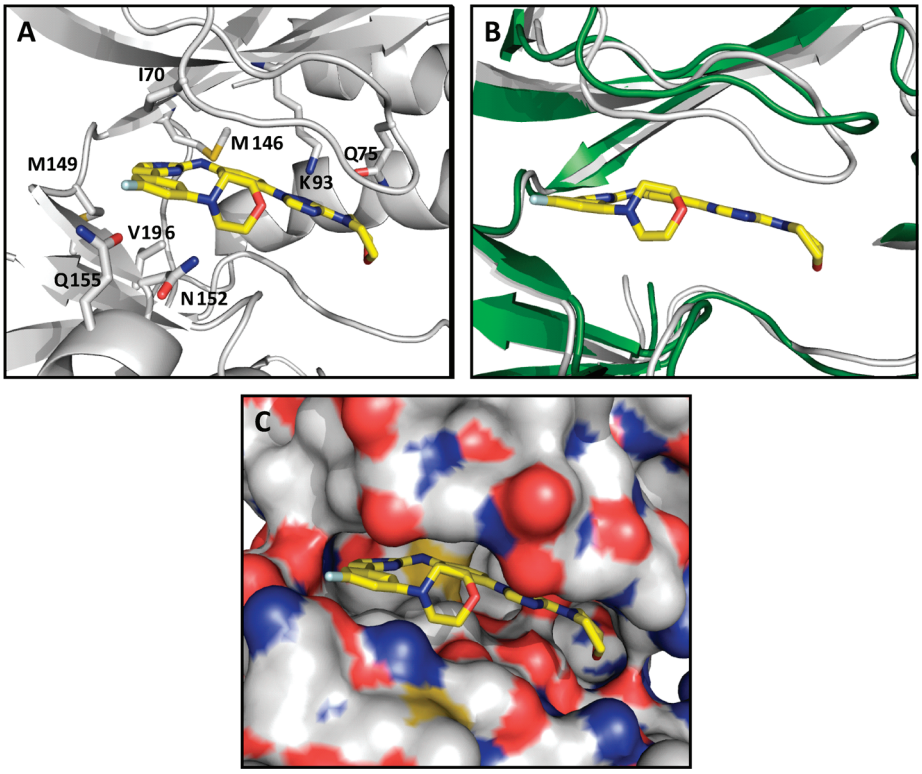

Figure 1. X-ray structure of JNK3 with compound **9l**. (A) The ATP binding pocket of JNK3 (gray) is shown in schematic ribbon form and key residues are shown stick form. Compound **9l** binding is shown. (B) Backbone trace of JNK3 (gray) complexed with compound **9l** overlaid with the backbone trace of JNK3 (green) from Scapin et al.[26] (C) Space filling model of JNK3 with compound **9l** bound.

Table 3. P450 Inhibition and Microsomal Stability of Key Aminopyrimidine JNK Inhibitors

	P450% Inhibition @ 10 μM[a]				
					microsomal stability[b] (min)
compd	2C9	2D6	3A4	1A2	mouse/rat/human
9f	43	4	48	39	5/17/18
9h	7	10	15	−1	26/11/17
9j	−2	−4	33	15	51/47/29
9l	75	4	89	70	21/41/26

[a] P450 inhibition assays examine the inhibition of selective marker reactions: CYP1A2 phenaceten (40 μM) → acetaminophen; CYP2C9, tolbutamide (130 μM) → hydroxytolbutamide; CYP2D6, bufuralol (40 μM) → 4′-hydroxybufuralol; CYP3A4, midazolam (5 μM) → 1′-hydroxymidazolam. [b] 2 mg/mL mouse, rat, or human liver microsomes were used in the stability studies.

P450 Inhibition and Microsomal Stability of Key Aminopyrimidines. Table 3 presents the cytochrome P450 inhibition of four human enzymes (2C9, 2D6, 3A4, and 1A2) at 10 μM compound along with the mouse, rat, and human microsomal stability. Compound **9f** showed < 50% inhibition for all four P450 enzymes but had relatively low microsomal stability, especially in mice (Table 3). Addition of the nitrile group to R3 and the tertrazole group to R4 in compound **9h** improved microsomal stability in mice to 26 min and reduced P450 inhibition to ≤15% for all four enzymes (Table 3). Compound **9j** had the best microsomal stability in all species for the four compounds highlighted and also had a good P450 inhibition profile with ≤33% inhibition for all four enzymes (Table 3). Compound **9l** had the worst P450 inhibition profile of the four compounds presented, with three of the four enzymes (2C9, 3A4, and 1A2) showing between 70 and 90% inhibition at 10 μM. However, the microsomal stability of **9l** for all three species was reasonable, rivaling that of **9j**, especially in rat and human (Table 3). We also determined the plasma protein binding for **9l** in mouse, rat, dog, monkey, and human (92%, 98%, 96%, 96%, and 92%, respectively).

Rat Pharmacokinetics and Mouse Brain Penetration for Key Aminopyrimidines. Table 4 presents the pharmacokinetic parameters for compounds dosed at 1 mg/kg iv and 2 mg/kg po in rats and the brain and plasma levels at 2 h of those same compounds dosed at 10 mg/kg ip in mice. Three of the four compounds had clearance rates ≤20 mL/min/kg with compound **9j**, having a very low Cl_p = 3 mL/min/kg (Table 4). Compound **9h** had the poorest overall pharmacokinetic properties with relatively high clearance (44 mL/min/kg), low oral exposure (AUC = 0.24 mM·h), and low oral bioavailability (%F = 14) (Table 4). Compound **9l** had the best oral bioavailability with %F = 45. Three of the four compounds showed brain:plasma ratios ≥50%, with compound **9h** having brain:plasma = 117%. Compound **9l** had the second best brain:plasma ratio at 75%, with compound 9**j** having the worst brain:plasma ratio at 10% (Table 4).

Inhibition of ROS Generated by STZ Treatment of INS-1 Cells by Compound 9l. To determine if the inhibitors had impact on JNK-mediated physiological responses, such as ROS generation, we examined STZ-induced ROS generation in INS-1 cells to be congruent with our phospho c-jun cell-based assays. Figure 2a presents the microscopic detection of ROS generated from INS-1 cells treated with STZ for 4 h in the absence or presence of seven concentrations of compound **9l**. Rotenone (data not shown) was used as a positive control for ROS generation and showed equivalent levels of ROS detected by the cell-permeable indicator 5-(and-6)-chloromethyl-2′,7′-dichlorofluorescin diacetate, acetyl ester

Table 4. Rat Pharmacokinetics and Mouse Brain Penetration of Key Aminopyrimidine JNK Inhibitors

	rat[a]						mouse[b] [μM]	
compd	Cl_p (mL/min/kg)	$t_{1/2}$ (h)	V_d (L/kg)	oral AUC (μM·h)	oral C_{max} (μM)	%F	[plasma]	[brain]
9f	10	0.8	0.4	2.0	0.95	25	11.2	6.2
9h	44	1.9	3.3	0.24	0.07	14	2.4	2.8
9j	3	3.0	0.6	5.9	0.5	27	1.0	0.1
9l	20	2.4	2.5	1.4	0.3	45	6.0	4.5

[a] 1 mg/kg iv; 2 mg/kg po. [b] 10 mg/kg ip 2 h.

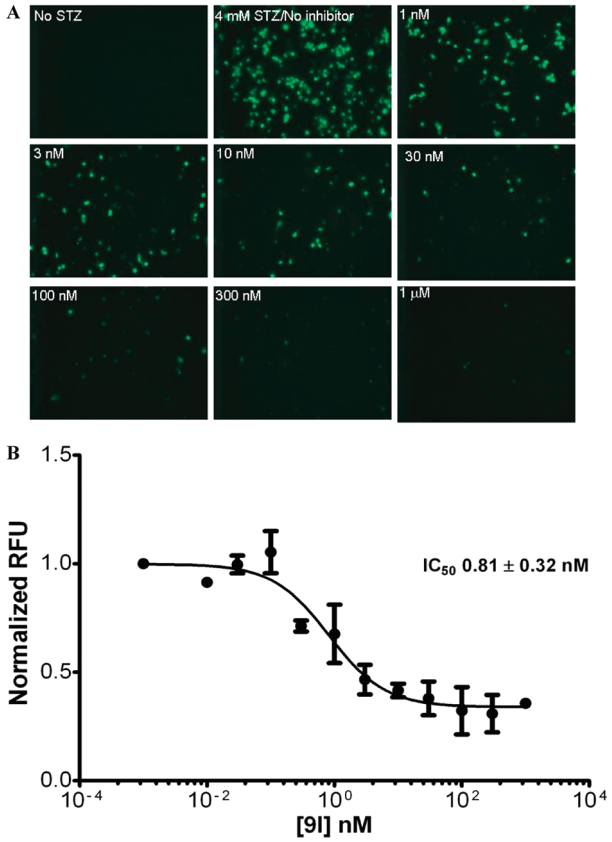

Figure 2. Compound **9l** inhibits STZ-induced intracellular ROS generation in INS-1 cells. (A) Fluorescent micrographs of H_2O_2 generation detected by H_2DCFDA. The absence of STZ treatment shows no ROS generation and 4 mM STZ treatment in the absence of compound **9l** shows maximum ROS generation. Seven concentrations of compound **9l** are shown in the presence of 4 mM STZ. (B) The normalized relative fluorescence units (RFU) for a 12-point dose response curve for compound **9l** is presented. The data are from four biological replicates with each dose repeated in duplicate. The IC_{50} presented is for the average of the four experiments ± the standard error of the mean (SEM).

(CM-H_2DCFDA), as was seen for the STZ only (panel 2 of Figure 2a). Figure 2b presents the IC_{50} determination of compound **9l** for the inhibition of ROS from the average of four biological replicates (with each concentration repeated in duplicate). These results showed a signal-to-background of three and that compound **9l** was a potent inhibitor of ROS generation in INS-1 cells.

Discussion

Given the strong preclinical validation for JNK as a target in neurodegenerative disease,[1−4] we set a goal of developing selective JNK inhibitors which were potent in cell-based assays, had good pharmacokinetic properties, and good brain penetration to make them viable candidates to probe in vivo neurodegenerative models. Thus, the SAR described in this report needed to balance all of these challenges.

Structure−Activity Relationships Affecting Biochemical and Cell-Based Potency for Aminopyrimidines. The key SAR element which gave rise to improved potency for both JNK3 and JNK1 in the biochemical assays was addition of the methyl sulfonamide at R2 to compounds **9d** and **9e** (Table 1). Indeed, compound **9e** was 91-fold more potent versus JNK3 than compound **9c** (which had H at R2) despite the fact that compound **9c** had the potency enhancing addition of the morpholino group at R1. Moreover, numerous analogues to compound **9e** were made containing alkyl, amide, amine, and morpholino substitutions (data not shown) at position R2 and none of these analogues had IC_{50}s nearly as potent as compound **9e**, suggesting that methyl sulfonamide substitution at this position was uniquely potency enhancing. It is unclear why compound **9e** is more potent than other analogues made. It is interesting to speculate that one reason compound **9e** was more potent than compound **9l** was that **9e** could potentially hydrogen bond to the backbone of Met 149 as seen for many JNK inhibitors, while compound **9l** as seen in Figure 1 did not have this interaction. A crystal structure of **9e** would be needed to address this hypothesis and see if other interactions such as H-bonding with Lys 93 or even Gln 155 or Asn 152 was possible for the sulfonamide moiety. Despite the improved biochemical potency of **9e** on JNK3 and JNK1, there was not an improved potency in the cell-based inhibition of c-jun phosphorylation assay owing to the relatively poor cell penetration of the methyl sulfonamides. This liability was further manifested in the brain penetration of methyl sulfonamide analogues, which showed very poor brain penetration. Improvements in cell potency came with addition of morpholino to R1 compared to H and addition of either morpholino or pyridyl substitutions on the triazole at R4. It is also likely that morpholino substitution at R1 contributed to enhanced solubility of compounds **9f**−**9l**.

The biochemical potency of the compounds described in Table 1 is similar to those seen for other aminopyrimidines reported.[18,19] The most potent phenyl-substituted pyrazolopyridine analogue of the aminopyrimidines (compound **30** in their manuscript) reported by Alam et al. had biochemical IC_{50}s for JNK2 and JNK3 at 5 nM, respectively, and 22 nM for JNK1.[18] This compares favorably to compounds **9e** (Table 1) in our work where IC_{50}s for JNK3 and JNK1 were 4 and 16 nM, respectively. It was suggested by Alam et al., by preliminary docking studies, that the phenyl group in compound **30** accessed the hydrophobic pocket in JNK3 and this contributed to the potency.[18] Confirmation of this was not reported by crystal structure work. The most striking difference between the aminopyrimidines reported in our current work compared to that of Alam et al.[18] is that despite the single digit nanomolar biochemical potency reported for compound **30**, the cell-based IC_{50} for inhibition of c-jun

phosphorylation was only 3.8 μM. This is 18-fold less potent than compound **9e** and 71-fold less potent than compound **9l** reported in our work (Table 1), suggesting better cell penetration of the triazole-substituted aminopyrimidines reported in this work. The 4-substituted-2-aminopyrimidines reported by Humphries et al. compare a little more favorably to the compounds reported in this manuscript, where a 4-OH-cycolhexyl analogue (compound **9c** from ref 19) had a biochemical IC_{50} versus JNK1 = 12 nM and a cell-based inhibition of c-jun phosphorylation = 98 nM.[19]

A broader comparison of the biochemical IC_{50}s against the benzothiazol-2-yl acetonitrile, JNK3 inhibitors, revealed that compound **9l** was equipotent (148 nM for compound **9l** vs 120 nM for AS601245 from Gaillard et al.[16]) and compound **9e** was 30-fold more potent than AS601245. It is difficult to compare cellular activities of these compounds because Gaillard et al. did not report cell-based IC_{50}s, but merely % inhibition at 10 μM compound, where they showed 90% inhibition of inteleukin-2 (IL-2) release in Jurkat cells at this concentration. In 2006, Szczepankiewicz et al. reported a series of aminopyridine-based JNK inhibitors which showed suitability for in vivo use. Of the many compounds reported, four were highlighted (compounds **6o**, **6s**, **18b**, and **35**) and they had cell-based IC_{50}s values = 920, 1300, 650, and 1750 nM, respectively. Compound **9l** was 12-fold more potent in cells than the most potent compound highlighted by Szczepankiewicz et al. and 32-fold more potent than the least potent compound highlighted.

While many of these JNK inhibitors have been characterized for selectivity against broad panels of kinases, few have reported the selectivity of these compounds versus p38α.[13,16] For the aminopyrimidines presented by Alam et al.,[18] the major focus for selectivity was versus CDK-2, so comparison of selectivity over p38 in their work cannot be made with the compounds reported here. Similarly, Humphries et al. did not report the IC_{50} for their compounds versus p38α but did do so for p38β, where they showed that compound **9c** was ~1000-fold selective over p38β.[19] If this selectivity holds for p38α as well, which one can speculate is highly likely, then the compounds presented by Humphries et al. compare favorably in their p38 selectivity to those reported in Table 1. The well described toxicity of p38 inhibitors necessitates this desired selectivity in any JNK inhibitor program.[27]

The lack of a shift in cell-based IC_{50} for compounds **9f**, **9g**, **9i**, **9j**, **9k**, and **9l** (Table 1) compared to biochemical IC_{50} versus JNK1 is of interest. In contrast to compound **9e**, which showed a 13-fold decrease in potency for the c-jun phosphorylation cell-based assay compared to the JNK1 biochemical IC_{50}, the aforementioned compounds were essentially equipotent in the biochemical and cell-based assays. One possible interpretation for the increased potency in the cells for these compounds could be that they have very slow off rates from the enzyme and hence have greater cell-based potency. This has been seen for other ATP competitive kinase inhibitors, including those for p38 where the biochemical and cell-based IC_{50}s were nearly identical.[21,28] It is less likely that there is another enzyme which phosphorylates c-jun in the cells, as very few enzymes beyond JNK have been reported to utilize c-jun as a substrate. Moreover, broad counterscreening of 3 μM **9l** against a panel of 400 kinases showed this class to be highly selective, with only 11 out of 400 kinases showing greater than 70% biochemical inhibition at this concentration and only 28 showing >25% inhibition. In addition, all of the upstream kinases which activate the JNK pathway were not inhibited at this concentration (MKK7, no inhibition; MKK4, no inhibition; MLK1−3, no inhibition, MAPK3K1−4, no inhibition, and ASK-1, no inhibition) by **9l**, further implicating direct JNK inhibition as the likely target in cells. Thus, inhibition of another putative enzyme which phosphorylates c-jun that was inhibited by the compounds in Table 1 is unlikely but cannot be strictly ruled out.

Crystallography of JNK3−Compound 9l Complex. The binding of compound **9l** to JNK3 was unique because of the lack of any hydrogen bonding in the structure, the significant contributions from hydrophobic interactions to the binding, the lack of movement of the gatekeeper Met 146, and the ~2.5 Å drop of the Gly-rich loop to compress the active site. A drop in the Gly-rich loop was not seen for the aminopyrimidines reported by Alam et al.,[18] where they showed more traditional type binding having hydrogen bonding interactions with Met 149 and steric interactions of a chlorine atom with gatekeeper Met 146 residue. Moreover, it appeared that compound **6** from Alam et al.[18] had key interactions with Gln 155, which were not present in the JNK3-compound **9l** structure presented in Figure 1. It is likely that the highly planar nature of compound **9l** is responsible for this movement of the Gly-rich loop as well as for the lack of the traditional interactions reported with Met 149 and Gln 155. Indeed, the highly planar compound **3** presented by Scapin et al. also showed a large drop in the position of the Gly-rich loop upon binding where the less planar compound **1** from that study did not show this drop.[26]

Swahn et al. showed that the anilino-bipyridines bound to JNK3 in the ATP pocket and were able to move the gatekeeper Met 146 by more than 2 Å, giving a few of these compounds selectivity for JNK3 over JNK1.[12] This movement of Met 146 was not seen for compound **9l**, nor was it seen for the compounds in the Alam et al. study and is likely the reason there is no selectivity for JNK3 over JNK1 for the compounds in Table 1. Attempts to utilize the Met 146 gatekeeper residue for improved potency and selectivity by substitution of our aminopyrimidines did not prove helpful.

P450 Inhibition and Microsomal Stability of Key Aminopyrimidines. Compounds **9h** and **9j** had the least P450 inhibition of any of the four compounds presented in Table 3. Addition of the CN group at R3 of compound **9h** was likely the major contributing factor to improving the inhibition profile versus 2C9, 3A4, and 1A2 compared to compound **9f**. Like **9h**, compound **9j** also contained CN at R3 and likely was the reason for low P450 inhibition of this compound too. Addition of the 3-pyridyl substitution to the triazole in **9j** further improved the P450 inhibition profile over a 3-morpholino substitution as seen in compound **9l**. These observations suggest a relatively strong interaction of the 3-morpholino substitution in compound **9l** with the P450s 2C9, 3A4, and 1A2, which was not found when pyridyl was at that position. While the 3-morpholino substitution was detrimental for P450 inhibition, this substitution enhanced microsomal stability in all species compared to simple methyl substitution of the triazole (compound **9f**). The same enhancement in microsomal stability was true for the pyridyl substitution. Both of these observations are consistent with the well-known ability of these groups to provide stability against liver microsomal metabolism of xenobiotics. The major liability of compound **9l** was the high P450 inhibition seen with the three enzymes noted in Table 3. Future SAR will be focused on improving this inhibition profile while still

maintaining all of the potency, selectivity, and PK properties of this series.

Rat Pharmacokinetics and Mouse Brain Penetration for Key Aminopyrimidines. Despite the favorable P450 profile and good microsomal stability of compound **9j**, it was found that this compound did not have good brain penetration compared to compounds **9f**, **9h**, and **9l** (Table 4). The poor brain penetration (brain:plasma ratio = 0.1) prohibited this compound from being considered for further assessment as a possible in vivo candidate in neurodegenerative models despite the good overall PK properties of the compound (Table 4). Brain penetration has been shown to be directly correlated with the polar surface area (PSA) of a compound (i.e., the lower the PSA, the greater the brain penetration).[29] Comparison of compound **9j**, which had a calculated PSA = 118 to compound **9l** which had a calculated PSA = 93, supported the experimental findings where compound **9l** had a brain:plasma ratio = 0.75. Compound **9l** also showed good rat pharmacokinetic parameters with good oral exposure (AUC = 1.4 mM·h at 2 mg/kg dose), good oral bioavailability (45%), and reasonable half-life (Table 4). It is likely that the combination of the fluoro substitution at R3, along with the 3-morpholino-1,2,4-triazole at R4 provided the balance needed for achieving good pharmacokinetic properties while maintaining the brain penetration needed to test neurodegenerative animal models. Indeed, it has been shown that polar surface area is positively correlated with both CNS exposure and oral bioavailability[30] and hence it is likely that compound **9l** strikes the balance needed for good permeability to cross the gut and blood−brain barrier, be stable against liver metabolism, as well as having potent cell inhibition of JNK. It should be mentioned that despite the very potent biochemical inhibition of JNK1 and JNK3 by compound **9e**, this compound was not pursued further because all of the methyl-sulfonamide substituted analogues we made had very poor brain penetration, which was likely associated with the very high polar surface area of these compounds (calculated PSA = 123 for compound **9e**). This compound also had $\%F = 5$, in keeping with the high PSA value and poor microsomal stability in all species.

Because none of the other JNK inhibitors reported were designed for CNS therapeutic indications, it is difficult to compare our compounds to the aminopyrimidines and other classes of compounds in the literature. It can be inferred, however, from the stated peripheral indications for these compounds that it is unlikely those compounds were optimized for brain penetration given the diabetes and inflammation indications cited for those programs.

Inhibition of ROS Generated by STZ Treatment of INS-1 Cells by Compound 9l. The potent inhibition of ROS generation ($IC_{50} = 0.81 \pm 0.32$ nM) by compound **9l** suggests that JNK has significant contribution to ROS generation in INS-1 cells. One potential explanation for this potency is that JNK activation (by STZ) induces ROS generation and therefore the inhibition of JNK prevents ROS generation. Thus even low levels of JNK inhibition may go a long way in preventing ROS generation. This possibility is supported by the findings of Davis and colleagues, who showed that TNFα-induced ROS production was JNK-dependent and that almost no ROS production, as measured by CM-H_2DCFDA detection, was seen in *jnk*−/− fibroblasts.[31] Similar findings were reported by Karin and colleagues, who also showed that TNFα-induced ROS production had a significant JNK dependence.[32] A second possibility comes from the significant role JNK plays in pathways which affect mitochondrial ROS generation. The major source of ROS in cells is the mitochondria.[33] Translocation of JNK to the mitochondria has been shown, and a possible role for the kinase in the organelle bioenergetics has been suggested.[34,35] Phosphorylation of mitochondrial proteins like Bcl-2, Bcl-XL, and Bax by JNK has been demonstrated, connecting JNK pathway directly with mitochondrial dependent apoptosis.[34−37] Hence, it is possible that inhibition of JNK not only decreases activation of the most well-known target of the kinase (c-jun) but it also inhibits a number of events that would irreversibly lead to disruption of the mitochondrial functions and cell death. Finally, despite the good selectivity profile of compound **9l**, it cannot be ruled out that off-target inhibition may contribute to some of the decreased ROS.

Summary and Conclusion

As in any medicinal chemistry program, multiple parameters need to be balanced to obtain a compound with the desired properties. CNS drugs in particular present a greater challenge, as one must incorporate brain penetration into the desired properties while still maintaining potency of the target of interest, selectivity, good microsomal stability, and good pharmacokinetic properties. In this report, we have managed to strike a balance of these properties by designing potent ATP-competitive JNK inhibitors which had cell-based IC_{50} values near 50 nM (compound **9l**) while maintaining a 200-fold selectivity over p38 and a broad set of kinases. This broad and high level of selectivity should help minimize potential side effects of these compounds. Moreover, these compounds have been shown to be highly brain penetrant while showing functional efficacy in reducing ROS production in cells. Given ROS production is a central mechanism for cell death in many neurodegenerative disorders, we feel that this class of aminopyrimidines represents good candidates for testing in vivo models of neurodegeneration. The major liability of compound **9l** is the high level of inhibition for some of the CYP450 enzymes. Future work will be focused on improving the CYP450 inhibition profile and trying to improve cell-based potency.

Experimental Section

Commercially available reagents and anhydrous solvents were used without further purification unless otherwise specified. Reactions were monitored by HPLC with YMC Pack-Pro C18 column (4.6 mm × 75 mm). Analytical HPLC data were generated by injecting 5 μL of very dilute sample solution in methanol or acetonitrile to a reverse phase HPLC system run over 14 min (5−95% acetonitrile/water with 0.1% TFA in each solvent). The products were detected by UV in the detection range of 215−310 nm. All compounds were determined to be >95% pure by this method. HRMS (electrospray ionization) experiments were performed with a Thermo Finnigan orbitrap mass analyzer. Data were acquired in the positive ion mode at a resolving power of 100000 at m/z 400. Calibration was performed with an external calibration mixture immediately prior to analysis. Thin layer chromatography (TLC) analyses were performed with precoated silica gel 60 F254. Flash chromatography was performed on prepacked columns of silica gel (230−400 mesh, 40−63 μm) by CombiFlash with EtOAc/hexane or $MeOH/CH_2Cl_2$ as eluent. The purification by preparative HPLC was performed on YMC Pack-Pro C18 column with CH_3CN + 50%$MeOH/H_2O$ + 0.1% TFA as eluent. The mass spectra were recorded by LCMS with the Finnigan LCQ Advantage MAX spectrometer of Thermo Electron. NMR spectra were recorded with a Bruker 400 MHz spectrometer at ambient temperature with the residual solvent

peaks as internal standards. The line positions of multiplets are given in ppm (δ).

4-(4-Phenylpyrimidin-2-ylamino)benzamide (9a).

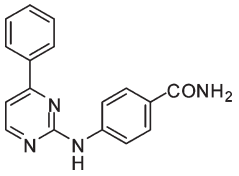

A mixture of 2-chloro-4-phenylpyrimidine (0.10 g, 0.52 mmol) (Combi-Blocks) and 4-aminobenzamide (0.21 g, 1.6 mmol) in 2-ethoxyethanol (3.0 mL) was heated in a sealed tube at 190 °C for 1 h (or at 120 °C overnight if aqueous 2-ethoxyethanol was used). The reaction mixture was cooled to room temperature and diluted with water. The precipitate was filtered, washed with water, and dried under air to provide the desired product as a tan solid >95% pure as judged by analytical HPLC analysis. q^{1}H NMR (DMSO-d_6, 400 MHz) δ 9.9 (s, 1H), 8.6 (d, 1H), 8.2 (br s, 2H), 7−7−8.0 (m, 5H), 7.6 (br s, 3H), 7.5 (d, 1H), 7.2 (br s, 1H). MS (ESI) 291.2 (M + H).

***N*-(4-(1*H*-1,2,4-Triazol-1-yl)phenyl)-4-phenylpyrimidin-2-amine (9b).**

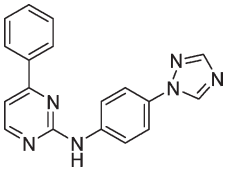

Compound **9b** was obtained following the same general protocol used in the preparation of compound **9a** using 2-chloro-4-phenylpyrimidine and 4-(1*H*-1,2,4-triazol-1-yl)aniline. ^{1}H NMR (DMSO-d_6, 400 MHz) δ 9.77 (s, 1H), 8.52 (dd, 1H), 8.34 (t, 1H), 8.14−8.10 (m, 2H), 7.92−7.88 (m, 2H), 7.73−7.70 (m, 2H), 7.64 (d, 1H), 7.53−7.48 (m, 2H), 7.37 (d, 1H), 6.45 (dd, 1H). MS (ESI) 315 (M + H).

***N*-(4-(1*H*-1,2,3-Triazol-1-yl)phenyl)-4-(3-morpholinophenyl)-pyrimidin-2-amine (9c).**

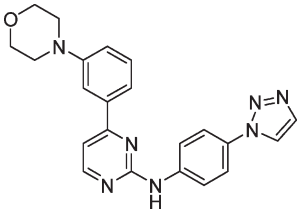

A mixture of 4-(3-(4,4,5,5-tetramethyl-1,3,2-dioxaborolan-2-yl)phenyl)morpholine (2.38 g, 8.23 mmol), 2,4-dichloropyrimidine (1.35 g, 9.05 mmol), Pd(PPh$_3$)$_4$ (0.48 g, 0.41 mmol), K_2CO_3 (12 mL of 2 M aq solution), and DME (24 mL) was purged with Ar for 10 min, then heated in a sealed tube at 90 °C overnight. The reaction mixture was cooled to room temperature and extracted with EtOAc (2×). The combined organics were dried ($MgSO_4$) and concentrated in vacuo to give an oil. Purification of this material by column chromatography on silica gel (25% EtOAc/hexane) provided 4-(3-(2-chloropyrimidin-4-yl)phenyl)morpholine as a yellow solid. ^{1}H NMR ($CDCl_3$, 400 MHz) δ 8.64 (d, 1H), 7.70 (s, 1H), 7.64 (d, 1H), 7.51−7.47 (m, 1H), 7.41 (t, 1H), 7.10−7.08 (m, 1H), 3.92−3.90 (m, 4H), 3.29−3.26 (m, 4H).

A mixture of 4-(3-(2-chloropyrimidin-4-yl)phenyl)morpholine was then coupled with 4-(1*H*-1,2,3-triazol-1-yl)aniline to give the title compound as described for compound **9a**. ^{1}H NMR (DMSO-d_6, 400 MHz) δ 9.98 (s, 1H), 8.74 (d, 1H), 8.59 (d, 1H), 8.09−8.05 (m, 2H), 7.86 (d, 1H), 7.86−7.82 (m, 2H), 7.76 (s, 1H), 7.65−7.62 (m, 1H), 7.52 (d, 1H), 7.42 (t, 1H), 7.16 (d, 1H), 3.81−3.79 (m, 4H), 3.25−3.23 (m, 4H). MS (ESI) 400 (M + H).

***N*-(4-(2-(4-(1*H*-1,2,3-Triazol-1-yl)phenylamino)pyrimidin-4-yl)-phenyl)methanesulfonamide (9e).**

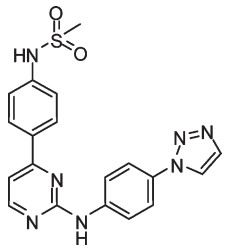

A mixture of *N*-(4-(4,4,5,5-tetramethyl-1,3,2-dioxaborolan-2-yl)phenyl)methanesulfonamide (0.85 g, 2.9 mmol), 2,4-dichloropyrimidine (0.84 g, 5.7 mmol), Pd(PPh$_3$)$_4$ (0.33 g, 0.29 mmol), Na_2CO_3 (5 mL of 2 M aq solution), and CH_3CN (15 mL) was purged with Ar for 10 min and then heated in a sealed tube at 90 °C overnight. The reaction mixture was cooled to room temperature and diluted with water and EtOAc. The layers were separated, and the aqueous layer was extracted with EtOAc (2×). The combined organics were dried ($MgSO_4$) and concentrated in vacuo to give a pale-yellow solid. Trituration of this solid with Et_2O provided *N*-(4-(2-chloropyrimidin-4-yl)phenyl)methanesulfonamide (0.60 g, 37%) which was used without further purification. ^{1}H NMR (DMSO-d_6, 400 MHz) δ 10.3 (br s, 1H), 8.8 (d, 1H), 8.2 (d, 2H), 8.1 (d, 1H), 7.3 (d, 2H), 3.1 (s, 3H).

The title compound was made following the general procedures described for compound **9a** using 4-(1*H*-1,2,3-triazol-1-yl)aniline. ^{1}H NMR ($CDCl_3$, 400 MHz) δ ^{1}H NMR (DMSO-d_6, 400 MHz) δ 10.18 (s, 1H), 9.96 (s, 1H), 8.74 (d, 1H), 8.58 (d, 1H), 8.19 (d, 2H), 8.07 (d, 2H), 7.95 (d, 1H), 7.85 (d, 2H), 7.43 (d, 1H), 7.37 (d, 2H), 3.32 (s, 6H), 3.12 (s, 3H). MS (ESI) 408.0 (M + H).

4-(4-(4-(Methylsulfonamido)phenyl)pyrimidin-2-ylamino)benzenesulfonamide (9d).

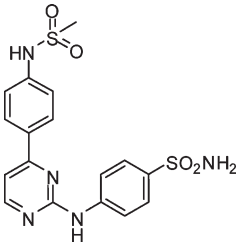

The title compound was made following the general procedures described for compound **9a** using *N*-(4-(2-chloropyrimidin-4-yl)phenyl)methanesulfonamide and 4-aminobenzenesulfonamide. ^{1}H NMR (DMSO-d_6, 400 MHz) δ 10.00 (s, 1H), 8.53 (d, 1H), 8.10 (d, 2H), 8.01 (d, 2H), 7.70 (d, 2H), 7.69−7.54 (m, 2H), 7.41 (d, 1H), 7.24 (d, 2H), 7.16 (s, 1H), 2.98 (s, 3H). MS (ESI) 420 (M + H).

***N*-(4-(3-Methyl-1*H*-1,2,4-triazol-1-yl)phenyl)-4-(3-morpholinophenyl)pyrimidin-2-amine (9f).**

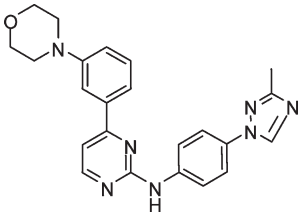

A mixture of 4-fluoro-1-nitrobenzene (0.77 g, 5.5 mmol), 3-methyl-1*H*-1,2,4-triazole (0.50 g, 6.0 mmol), K_2CO_3 (0.83 g,

6.0 mmol), and DMF (25 mL) was heated at 75 °C overnight. The reaction mixture was cooled to room temperature, diluted with water, and extracted with EtOAc (3×). The organic layer was dried ($MgSO_4$) and concentrated to provide a solid. Purification of this material by column chromatography on silica gel (40% EtOAc/hexane) provided 3-methyl-1-(4-nitrophenyl)-1*H*-1,2,4-triazole as the major product. ^{1}H NMR ($CDCl_3$, 400 MHz) δ 8.59 (s, 1H), 8.39 (d, 2H), 7.88 (d, 2H), 2.53 (s, 3H). MS (ESI) 205.1 (M + H). HRMS, MH^+: calculated for $C_{23}H_{23}N_7O$ 414.20366; obtained 414.2038.

A mixture of 3-methyl-1-(4-nitrophenyl)-1*H*-1,2,4-triazole (0.24 g, 1.2 mmol), 5% Pt/C, and MeOH (12 mL) was stirred at room temperature under H_2 balloon overnight. The reaction mixture was filtered through celite and concentrated in vacuo to provide the desired product as a beige solid which was used without further purification. ^{1}H NMR ($CDCl_3$, 400 MHz) δ 8.31 (s, 1H), 7.40 (d, 2H), 6.77 (d, 2H), 2.51 (s, 3H).

The title compound was made following the general procedure described for compound **9a** using 4-(3-(2-chloropyrimidin-4-yl)phenyl)morpholine and 4-(3-methyl-1*H*-1,2,4-triazol-1-yl)aniline. ^{1}H NMR ($CDCl_3$, 400 MHz) δ 8.42 (d, 1H), 8.31 (s, 1H), 7.80 (d, 2H), 7.67 (s, 1H), 7.59 (d, 2H), 7.46 (d, 1H), 7.34 (t, 1H), 7.13 (d, 1H), 7.01 (d, 1H), 3.86−3.84 (m, 4H), 3.21−3.19 (m, 4H), 2.44 (s, 3H). MS (ESI) 414.25 (M + H).

3-(2-(4-(3-Methyl-1*H*-1,2,4-triazol-1-yl)phenylamino)pyrimidin-4-yl)-5-morpholinobenzonitrile (9g).

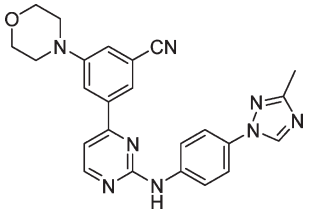

A mixture of 3-bromo-5-fluorobenzonitrile (5.4 g, 27.0 mmol) and morpholine (100 mL) was heated in a sealed tube at 120 °C overnight. When the reaction was done as judged by analytical HPLC analysis, the reaction was cooled to room temperature and quenched with water (400 mL). The resulting colorless precipitate was collected by filtration, dried in vacuo, and used without further purification. ^{1}H NMR ($CDCl_3$, 400 MHz) δ 7.25 (s, 1H), 7.24 (s, 1H), 7.07 (t, 1H), 3.88 (t, 4H), 3.22 (t, 4H). MS (ESI) 267.1, 269.1 (Br isotope) (M + H).

A mixture of 3-bromo-5-morpholinobenzonitrile (4 g, 15.0 mmol), bis(pinacolato)diboron (5.0 g, 19.5 mmol), Pd(dppf)Cl_2-(CH_2Cl_2) (0.68 g, 0.75 mmol), KOAc (4.4 g, 45.0 mmol), and DMSO (30 mL) was degassed with argon and then heated in a sealed tube at 100 °C for 6 h. The reaction mixture was cooled to room temperature, diluted with water, and extracted with ethyl acetate (2×). The combined organics were dried ($MgSO_4$), filtered through a short pad of silica gel, and concentrated to give the borate as a tan solid, which was used without further purification. ^{1}H NMR ($CDCl_3$, 400 MHz) δ 7.49 (s, 1H), 7.45 (d, 1H), 7.10−7.09 (m, 1H), 3.79 (t, 4H), 3.14 (t, 4H), 1.19 (s, 12H). MS (ESI) 315.2 (M + H).

A mixture of this borate (3.6 g, 11.5 mmol), 2,4-dichloropyrimidine (2.2 g, 14.9 mmol), Pd(PPh_3)$_4$ (0.66 g, 0.6 mmol), K_2CO_3 (20 mL of 2 M aq. solution), and DME (40 mL) was purged with Ar for 10 min and then heated in a sealed tube at 95 °C for 12 h. The reaction mixture was cooled to room temperature, diluted with water and EtOAc, and the layers were separated. The aqueous layer was extracted with EtOAc (2×). The combined organics were dried ($MgSO_4$) and concentrated in vacuo to give a pale-yellow solid that was used without further purification. ^{1}H NMR ($CDCl_3$, 400 MHz) δ 8.73 (d, 1H), 7.91−7.90 (m, 1H), 7.73−7.72 (m, 1H), 7.65 (d, 1H), 7.27−7.26 (m, 1H), 3.93−3.91 (m, 4H), 3.34−3.31 (m, 4H). MS (ESI) 301.1 (M + H).

Compound **9g** was prepared from this crude 2-chloropyrimidine and 4-(3-methyl-1*H*-1,2,4-triazol-1-yl)aniline as previously described for compound **9a**. ^{1}H NMR (DMSO-d_6, 400 MHz) δ 9.95(s, 1H), 9.05 (s, 1H), 8.64 (d, 1H), 8.02−7.92 (m, 3H), 7.74 (d, 2H), 7.60−7.55 (m, 2H), 3.81−3.78 (m, 4H), 3.34−3.29 (m, 4H). MS (ESI) 439 (M + H).

3-(2-(4-(2-Methyl-2*H*-tetrazol-5-yl)phenylamino)pyrimidin-4-yl)-5-morpholinobenzonitrile (9h).

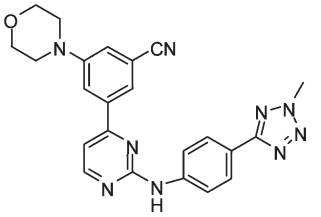

A mixture of 4-(2*H*-tetrazol-5-yl)aniline (1.13 g, 7.0 mmol), MeI (1.09 g, 7.7 mmol), and K_2CO_3 (1.93 g, 14.0 mmol) in acetone (14 mL) was stirred at 40 °C for 1 h. The reaction mixture was filtered, and the filtrate was concentrated in vacuo to give a solid. Purification of this material by column chromatography on silica gel (40% EtOAc/hexane) provided 4-(2-methyl-2*H*-tetrazol-5-yl)aniline as a white solid. ^{1}H NMR ($CDCl_3$, 400 MHz) δ 7.94 (d, 2H), 6.77 (d, 2H), 4.37 (s, 3H), 3.90 (brs, 2H).

A mixture of 3-(2-chloropyrimidin-4-yl)-5-morpholinobenzonitrile (0.040 g, 0.13 mmol) and 4-(2-methyl-2*H*-tetrazol-5-yl)aniline (0.024 g, 0.13 mmol) in 2-ethoxyethanol (0.2 mL) was heated in a sealed tube at 190 °C for 1 h. The reaction mixture was cooled to room temperature and diluted with water. The precipitate was filtered, washed with water, and dried under air to provide 3-(2-(4-(2-methyl-2*H*-tetrazol-5-yl)phenylamino)pyrimidin-4-yl)-5-morpholinobenzonitrile as a brown solid. ^{1}H NMR ($CDCl_3$, 400 MHz) δ 8.49 (d, 1H), 8.05 (d, 2H), 7.86 (s, 1H), 7.76 (d, 2H), 7.65 (s, 1H), 7.36 (s, 1H), 7.16 (d, 1H), 7.10 (d, 1H), 4.33 (s, 3H), 3.86−3.84 (m, 4H), 3.24−3.22 (m, 4H). MS (ESI) 440.11 (M + H). HRMS, MH^+: calculated for $C_{23}H_{21}N_9O$, 440.19414; obtained, 440.1941.

4-(3-Morpholinophenyl)-*N*-(4-(3-(pyridin-3-yl)-1*H*-1,2,4-triazol-1-yl)phenyl)pyrimidin-2-amine (9i).

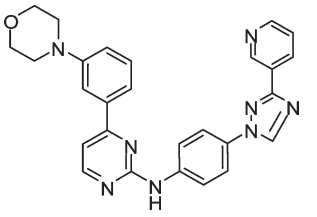

3-Bromo-1-(4-nitrophenyl)-1*H*-1,2,4-triazole was obtained from 3-bromo-1*H*-1,2,4-triazole and 4-fluoro-1-nitrobenzene as described for compound **9g**. ^{1}H NMR ($CDCl_3$, 400 MHz) δ 8.60 (s, 1H), 8.44 (d, 2H), 7.91 (d, 2H).

A mixture of 3-bromo-1-(4-nitrophenyl)-1*H*-1,2,4-triazole (0.51 g, 1.9 mmol), $SnCl_2$-$2H_2O$ (2.14 g, 9.5 mmol), and EtOH (4 mL) was heated at reflux for 4 h. The reaction mixture was cooled to room temperature and basified with NaOH (2 M aq) until pH 7−9. The resulting precipitate was filtered through celite and washed with EtOH. The EtOH filtrate was concentrated in vacuo, and the crude residue was dissolved in water and extracted with EtOAc (3×). The combined organics were dried ($MgSO_4$) and concentrated in vacuo to provide the desired product as a white solid. ^{1}H NMR ($CDCl_3$, 400 MHz) δ 8.28 (s, 1H), 7.40 (d, 2H), 6.79 (d, 2H), 3.90 (br s, 2H).

A mixture of 4-(3-(2-chloropyrimidin-4-yl)phenyl)morpholine (0.11 g, 0.40 mmol) and 4-(3-bromo-1*H*-1,2,4-triazol-1-yl)aniline (0.12 g, 0.48 mmol) in 2-ethoxyethanol (2 mL)/water

(1 mL) was heated in a sealed tube at 120 °C overnight. The reaction mixture was cooled to room temperature and diluted with water. The precipitate was filtered, washed with water, and dried under air to provide *N*-(4-(3-bromo-1*H*-1,2,4-triazol-1-yl)phenyl)-4-(3-morpholinophenyl)pyrimidin-2-amine as a brown solid. ^{1}H NMR ($CDCl_3$, 400 MHz) δ 8.53 (d, 1H), 8.40 (s, 1H), 7.92 (d, 2H), 7.69 (s, 1H), 7.62 (d, 2H), 7.55 (d, 1H), 7.44 (t, 1H), 7.37 (s, 1H), 7.24 (s, 1H), 7.12 (d, 1H), 3.95−3.93 (m, 4H), 3.31−3.29 (m, 4H). MS (ESI) 478.17 and 480.20 (M + H).

A mixture of *N*-(4-(3-bromo-1*H*-1,2,4-triazol-1-yl)phenyl)-4-(3-morpholinophenyl)pyrimidin-2-amine (0.034 g, 0.07 mmol), pyridin-3-ylboronic acid (0.017 g, 0.14 mmol), K_2CO_3 (0.058 g, 0.42 mmol), $Pd(PPh_3)_4$ (0.008 g, 0.007 mmol), toluene (0.40 mL), and MeOH (0.10 mL) was heated in a sealed tube at 120 °C with microwave irradiation for 1 h. The reaction mixture was cooled down to room temperature and filtered. The filtrate was concentrated to a yellow solid. Purification of this material by column chromatography on silica gel (80% EtOAc/hexane) provided 4-(3-morpholinophenyl)-*N*-(4-(3-(pyridin-3-yl)-1*H*-1,2,4-triazol-1-yl)phenyl)pyrimidin-2-amine as a white yellow solid. ^{1}H NMR ($CDCl_3$, 400 MHz) δ 9.37 (br s, 1H), 8.60 (brs, 1H), 8.48 (s, 1H), 8.44 (d, 1H), 8.39 (d, 1H), 7.83 (d, 2H), 7.64−7.60 (m, 3H), 7.50 (s, 1H), 7.46 (d, 1H), 7.35−7.34 (m, 2H), 7.14 (d, 1H), 7.00 (dd, 1H), 3.84−3.82 (m, 4H), 3.20−3.18 (m, 4H). MS (ESI) 477.34 (M + H).

3-Morpholino-5-(2-(4-(3-(pyridin-2-yl)-1*H*-1,2,4-triazol-1-yl)-phenylamino)pyrimidin-4-yl)benzonitrile (9j).

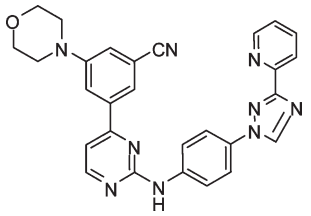

A mixture of 3-bromo-1-(4-nitrophenyl)-1*H*-1,2,4-triazole (2.15 g, 8.0 mmol), 2-(tributylstannyl)pyridine (4.42 g, 12.0 mmol), $Pd(PPh_3)_4$ (0.46 g, 0.40 mmol), and toluene (32 mL) was heated in a sealed tube at 130 °C overnight. The reaction mixture was cooled to room temperature, diluted with saturated aqueous $NaHCO_3$ and EtOAc, and the layers were separated. The aqueous layer was extracted with EtOAc (2×). The combined organics were dried ($MgSO_4$) and concentrated in vacuo to give 2-(1-(4-nitrophenyl)-1*H*-1,2,4-triazol-3-yl)pyridine as a brown solid that was used without further purification. ^{1}H NMR ($CDCl_3$, 400 MHz) δ 8.83−8.81 (m, 1H), 8.79 (s, 1H), 8.43 (d, 2H), 8.27 (d, 1H), 8.06 (d, 2H), 7.87 (t, 1H), 7.43−7.39 (m, 1H).

4-(3-(Pyridin-2-yl)-1*H*-1,2,4-triazol-1-yl)aniline was obtained following hydrogenation of 2-(1-(4-nitrophenyl)-1*H*-1,2,4-triazol-3-yl)pyridine as described for compound **9f**. ^{1}H NMR ($CDCl_3$, 400 MHz) δ 8.78−8.76 (m, 1H), 8.49 (s, 1H), 8.22 (d, 1H), 7.84−7.82 (m, 1H), 7.55 (d, 2H), 7.36−7.32 (m, 1H), 6.78 (d, 2H), 3.86 (brs, 2H).

3-Morpholino-5-(2-(4-(3-(pyridin-2-yl)-1*H*-1,2,4-triazol-1-yl)phenylamino)pyrimidin-4-yl)benzonitrile was prepared following the same general protocol as described for compound **9a** using 3-(2-chloropyrimidin-4-yl)-5-morpholinobenzonitrile (0.060 g, 0.20 mmol) and 4-(3-(pyridin-2-yl)-1*H*-1,2,4-triazol-1-yl)aniline (0.047 g, 0.20 mmol). ^{1}H NMR (DMSO-d_6, 400 MHz) δ 10.03 (s, 1H), 9.33 (s, 1H), 8.73−8.72 (m, 1H), 8.67 (d, 1H), 8.17 (d, 1H), 8.03−7.97 (m, 5H), 7.89 (d, 2H), 7.62 (d, 1H), 7.57 (s, 1H), 7.51−7.50 (m, 1H), 3.81−3.79 (m, 4H), 3.34−3.32 (m, 4H). MS (ESI) 502.38 (M + H). HRMS, MH^+: calculated for $C_{28}H_{23}N_9O$, 502.20979; obtained, 502.2102.

4-(3-Fluoro-5-morpholinophenyl)-*N*-(4-(3-(4-methylpiperazin-1-yl)-1*H*-1,2,4-triazol-1-yl)phenyl)pyrimidin-2-amine (9k).

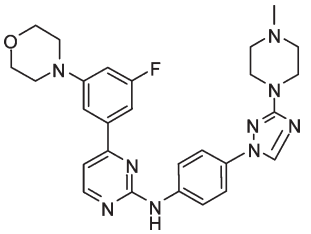

A mixture of 1-bromo-3,5-difluorobenzene (8.0 g, 41.5 mmol) in morpholine (100 mL) was heated in a sealed tube at 120 °C for 30 h and then concentrated in vacuo. The resulting residue was dissolved in EtOAc and washed with saturated aqueous NaHCO3 (2×), brine (1×), dried (MgSO4), and concentrated. The resulting pale-yellow oil slowly crystallized and was judged to be >90% pure by analytical HPLC analysis. It was used without further purification.

A mixture of 4-(3-bromo-5-fluorophenyl)morpholine (4.38 g, 16.8 mmol), bis(pinacolato)diboron (5.56 g, 21.9 mmol), Pd-(dppf)$Cl_2(CH_2Cl_2)$ (0.69 g, 0.84 mmol), KOAc (4.96 g, 50.5 mmol), and DMSO (17 mL) was purged with Ar for 3 min and then heated in a sealed tube at 100 °C overnight. The reaction mixture was cooled to room temperature, diluted with water, and extracted with ethyl acetate (2×). The combined organics were dried ($MgSO_4$), filtered through a short pad of silica gel, and concentrated to provide an oil. Purification of this material by column chromatography on silica gel (10% EtOAc/hexane) provided 4-(3-fluoro-5-(4,4,5,5-tetramethyl-1,3,2-dioxaborolan-2-yl)phenyl)morpholine as a white solid. ^{1}H NMR ($CDCl_3$, 400 MHz) δ 7.14 (s, 1H), 7.06−6.99 (m, 1H), 6.71−6.66 (m, 1H), 3.88−3.86 (m, 4H), 3.22−3.20 (m, 4H), 1.37 (s, 12H).

4-(3-(2-Chloropyrimidin-4-yl)-5-fluorophenyl)morpholine was prepared from 2,4-dicholorpyrimidine and 4-(3-fluoro-5-(4,4,5,5-tetramethyl-1,3,2-dioxaborolan-2-yl)phenyl)morpholine as described for compound **9g**. Purification by chromatography on silica gel (20% EtOAc/hexanes) provided the coupled product as a yellow solid. ^{1}H NMR ($CDCl_3$, 400 MHz) δ 8.67 (d, 1H), 7.60 (d, 1H), 7.52−7.51 (m, 1H), 7.24−7.21 (m, 1H), 6.81−6.77 (m, 1H), 3.93−3.86 (m, 4H), 3.31−3.28 (m, 4H).

A mixture of 4-(3-(2-chloropyrimidin-4-yl)-5-fluorophenyl)-morpholine was prepared from 2,4-dicholorpyrimidine was treated with 4-(3-bromo-1*H*-1,2,4-triazol-1-yl)aniline as described for compound **9g** to give *N*-(4-(3-bromo-1*H*-1,2,4-triazol-1-yl)phenyl)-4-(3-fluoro-5-morpholinophenyl)pyrimidin-2-amine after precipitation from the reaction mixture. ^{1}H NMR (DMSO-d_6, 400 MHz) δ 10.00 (s, 1H), 9.23 (s, 1H), 8.62 (d, 1H), 8.01 (d, 2H), 7.75 (d, 2H), 7.59 (s, 1H), 7.55 (d, 1H), 7.40−7.39 (m, 1H), 7.01−7.00 (m, 1H). MS (ESI) 496.17 and 498.17 (M + H).

This crude residue was treated with 1-methylpiperazine in the presence of K_2CO_3 with DMSO as the solvent at 190 °C overnight. The crude reaction was subjected to reverse-phase prep-HPLC purification to give compound **9k** as a yellow solid. ^{1}H NMR ($CDCl_3$, 400 MHz) δ 10.70 (brs, 1H), 8.28 (d, 1H), 8.19 (s, 1H), 7.78 (d, 2H), 7.52 (d, 2H), 7.34 (s, 1H), 7.17 (d, 1H), 7.13 (d, 1H), 6.73 (dd, 1H), 4.18−4.17 (m, 2H), 3.82−3.80 (m, 4H), 3.57−3.55 (m, 2H), 3.50−3.48 (m, 2H), 3.19−3.17 (m, 4H), 2.89−2.87 (m, 2H), 2.79 (s, 3H). MS (ESI) 516.34 (M + H).

4-(3-Fluoro-5-morpholinophenyl)-*N*-(4-(3-morpholino-1*H*-1,2,4-triazol-1-yl)phenyl)pyrimidin-2-amine (9l).

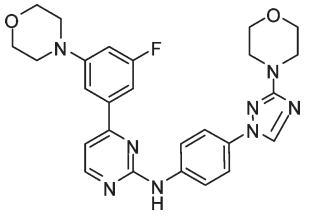

A mixture of 3-bromo-1-(4-nitrophenyl)-1*H*-1,2,4-triazole (1.35 g, 5.0 mmol) and morpholine (8.71 g, 100 mmol) was heated in a sealed tube at 120 °C overnight. The reaction mixture was cooled down to room temperature and diluted with water. The precipitate was filtered, washed with water, and dried under air to provide the desired product as a brown solid. ^{1}H NMR ($CDCl_3$, 400 MHz) δ 8.40 (s, 1H), 8.34 (d, 2H), 7.80 (d, 2H), 3.85−3.83 (m, 4H), 3.55−3.53 (m, 4H). MS (ESI) 276.13 (M + H).

4-(3-Morpholino-1*H*-1,2,4-triazol-1-yl)aniline was obtained following hydrogenation of 4-(1-(4-nitrophenyl)-1*H*-1,2,4-triazol-3-yl)morpholine as described for compound **9f**. ^{1}H NMR ($CDCl_3$, 400 MHz) δ 8.10 (s, 1H), 7.38 (d, 2H), 6.75 (d, 2H), 3.87−3.85 (m, 4H), 3.80 (br s, 2H), 3.52−3.50 (m, 4H). MS (ESI) 246.17 (M + H).

A mixture of 4-(3-(2-chloropyrimidin-4-yl)-5-fluorophenyl)morpholine (0.103 g, 0.35 mmol) and 4-(3-morpholino-1*H*-1,2,4-triazol-1-yl)aniline (0.086 g, 0.35 mmol) in 2-ethoxyethanol (0.5 mL) was heated in a sealed tube at 190 °C for 1 h. The reaction mixture was cooled to room temperature and diluted with water. The precipitate was filtered, washed with water, and dried under air to provide compound **9l** as a brown solid. ^{1}H NMR ($CDCl_3$, 400 MHz) δ 8.45 (d, 1H), 8.13 (s, 1H), 7.72 (d, 2H), 7.49 (d, 2H), 7.37 (s, 1H), 7.36 (s, 1H), 7.14 (d, 1H), 7.07 (d, 1H), 6.65 (d, 1H), 3.83−3.81 (m, 4H), 3.79−3.77 (m, 4H), 3.45−3.43 (m, 4H), 3.19−3.17 (m, 4H). MS (ESI) 503.31 (M + H). HRMS, MH^+: calculated for $C_{26}H_{27}FN_8O_2$, 503.23134; obtained, 503.2317.

Expression and Purification of JNK3 and ATF2. JNK3 and ATF2 were expressed and purified as described by Kamenecka et al.[11] JNK1 and p38 were purchased from Millipore.

Homogeneous Time Resolved Fluoresence Assay for JNK1, JNK3, and p38 Biochemical Assays. The assays were run as described by Kamenecka et al.[11] JNK3 expression in human, and rat pancreas, and insulin secreting INS-1 cells has been reported.[38]

Cell-Based Assay Measuring JNK Activity. Inhibition of c-jun phosphorylation in INS-1 β-pancreatic cells was run as described by Kamenecka et al.[11]

Cell-Based Assay Measuring Reactive Oxygen Species Generation in INS-1 β-Pancreatic Cells. Rat insulinoma cells (INS-1 823/13) were plated in 6-well plates (5×10^5−1×10^6 cells/well) in RPMI 1640 containing 10% fetal bovine serum (FBS). Cells were incubated overnight at 37 °C in 5% CO_2 and 95% humidity. Cells were treated with compound **9l** dissolved in dimethyl sulfoxide (DMSO) for 30 min prior to the administration of 4 mM streptozotocin (STZ) solubilized in medium. Inhibitors were present during STZ stimulation at the same concentrations used during the 30 min pre-STZ step. Cells were incubated with STZ for 4 h at 37 °C. Cells were washed twice with red phenol free RPMI 1640 containing 10% FBS. Detection of ROS generated in INS1 cells during treatments was done by oxidation (by H_2O_2) of the cell-permeable indicator 5-(and-6)-chloromethyl-2′,7′-dichlorofluorescin diacetate, acetyl ester (CM-H_2DCFDA; Invitrogen, Carlsbad, CA). The ROS indicator was prepared in red phenol free RPMI 1640 at 5 μM, added to cells and incubated for 1 h at 37 °C. Stained cells were resuspended and washed twice by centrifugation (5 min at room temperature) using red phenol free RPMI 1640 medium. Quantification of generated ROS was done in a microplate reader Spectramax M5e (Molecular Devices, Sunnyvale, CA) using a 96-well black plate with clear bottom (Perkin-Elmer, Whaltham, MA); 10^5 cells were transferred to each well in a 200 μL volume of red phenol free medium. Excitation of the fluorescein probe was done at 495 nm and emission was recorded at 525 nm. Control treatments included DMSO treated cells (no ROS control) and 10 μM rotenone for 1 h (ROS positive control). The normalized relative fluorescence units (RFU) were calculated for each point by dividing the obtained RFU by the RFU value corresponding to the STZ-treated INS-1 cells in the absence of inhibitor. The IC_{50} determined was from the averages of four biological replicates with each concentration repeated in duplicate. The data were fitted by nonlinear regression of the four-parameter equation.

Crystallization of JNK3. JNK3 was crystallized as described by Kamenecka et al.[11] and compound **9l** was soaked into the crystals over 36 h.

Data Collection and Structure Solution of JNK3-9l. Liquid nitrogen cooled crystals were loaded into an SSRL cassette for shipping. Data was collected remotely at SSRK on beamline 9−1.[39] Data sets were indexed, integrated, and scaled to the orthorhombic spacegroup $C222_1$ using HKL2000.[40] Initial phases were determined via molecular replacement, with PDB ID 1JNK as the search model, using PHASER.[41] The initial model was refined by alternating cycles of restrained refinement using REFMAC5[42] and manual model building using COOT.[43] PHASER and REFMAC5 are part of the CCP4[44] suite of software. Model geometry, bond lengths, and steric clashes were monitored using MOLPROBITY.[45] The ligand was placed into positive density in $F_o - F_c$ electron density map. Figures and rmsd values were generated using PYMOL.[46]

P450 Inhibition and Microsomal Stability Assays. P450 inhibition for the four major human isoforms was evaluated by following the metabolism of specific marker substrates (CYP1A2 phenaceten demethylation to acetaminophen; CYP2C9, tolbutamide hydroxylation to hydroxytolbutamide; CYP2D6, bufuralol hydroxylation to 4′-hydroxybufuralol; and CYP3A4, midazolam hydroxylation to 1′-hydroxymidazolam) in the presence or absence of 10 μM test compound for 15 min at 37 °C. The concentration of each marker substrate was approximately its K_m. Specific inhibitors for each isoform were included in each run to validate the system. Microsome (mouse, rat, human; Xenotech, Lenexa, Kansas) stability was evaluated by incubating 1 μM test compound with 2 mg/mL hepatic microsomes in 100 mM KPi, pH 7.4. The reaction was initiated at 37 °C by adding NADPH (1 mM final concentration). Aliquots were removed at 0, 5, 10, 20, 40, and 60 min and added to acetonitrile (5× v:v) to stop the reaction and precipitate the protein. At the end of the assay, the samples were centrifuged through a Millipore Multiscreen Solvinter 0.45 μm low binding polytetrafluoroethylene (PTFE) hydrophilic filter plate and analyzed by LC-MS/MS. Data was log transformed and regression analysis was used to calculate half-life.

Rat Pharmacokinetics and Mouse Brain Penetration. Pharmacokinetics of test compounds was assessed in Sprague−Dawley rats ($n = 3$). Compounds were dosed intravenously at 1 mg/kg and orally by gavage at 2 mg/kg. Blood was taken at eight time points (5, 15, 30 min, 1, 2, 4, 6, 8 h) and collected into EDTA containing tubes and plasma was generated using standard centrifugation techniques. Plasma proteins were precipitated with acetonitrile and drug concentrations were determined by LC-MS/MS. Data was fit by WinNonLin using a noncompartmental model and basic pharmacokinetic parameters including peak plasma concentration (C_{max}), oral bioavailability, exposure (AUC), half-life ($t_{1/2}$), clearance (CL), and volume of distribution (V_d) were calculated.

CNS exposure was evaluated in C57Bl6 mice ($n = 3$). Compounds were dosed at 10 mg/kg intraperitoneally and after 2 h blood and brain were collected. Plasma was generated and the samples were frozen at −80 °C. The plasma and brain were mixed with acetonitrile (1:5 v:v or 1:5 w:v, respectively). The brain sample was sonicated with a probe tip sonicator to break up the tissue, and samples were analyzed for drug levels by LC-MS/MS. Plasma drug levels were determined against standards made in plasma and brain levels against standards made in blank brain matrix. All procedures were approved by the Scripps Florida IACUC.

Acknowledgment. This work was supported by NIH grant U01-NS057153 awarded to P.L. Portions of this research were carried out at the Stanford Synchrotron Radiation Laboratory, a national user facility operated by Stanford University

on behalf of the U.S. Department of Energy, Office of Basic Energy Sciences. The SSRL Structural Molecular Biology Program is supported by the Department of Energy, Office of Biological and Environmental Research, and by the National Institutes of Health, National Center for Research Resources, Biomedical Technology Program, and the National Institute of General Medical Sciences. We are grateful to Dr. Mike Chalmers for HRMS determination and Yamille Del Rosario for administrative assistance in preparing the manuscript. INS-1 cells were a kind gift from Dr. Christopher Newgard at Duke University.

References

(1) Xia, X. G.; Harding, T.; Weller, M.; Bieneman, A.; Uney, J. B.; Schulz, J. B. Gene transfer of the JNK interacting protein-1 protects dopaminergic neurons in the MPTP model of Parkinson's disease. *Proc. Natl. Acad. Sci. U.S.A* **2001**, *98*, 10433–10438.

(2) Hunot, S.; Vila, M.; Teismann, P.; Davis, R. J.; Hirsch, E. C.; Przedborski, S.; Rakic, P.; Flavell, R. A. JNK-mediated induction of cyclooxygenase 2 is required for neurodegeneration in a mouse model of Parkinson's disease. *Proc. Natl. Acad. Sci. U.S.A* **2004**, *101*, 665–670.

(3) Borsello, T.; Clarke, P. G.; Hirt, L.; Vercelli, A.; Repici, M.; Schorderet, D. F.; Bogousslavsky, J.; Bonny, C. A peptide inhibitor of c-Jun N-terminal kinase protects against excitotoxicity and cerebral ischemia. *Nat. Med.* **2003**, *9*, 1180–1186.

(4) Pirianov, G.; Brywe, K. G.; Mallard, C.; Edwards, A. D.; Flavell, R. A.; Hagberg, H.; Mehmet, H. Deletion of the c-Jun N-terminal kinase 3 gene protects neonatal mice against cerebral hypoxic-ischaemic injury. *J. Cereb. Blood Flow Metab.* **2007**, *27*, 1022–1032.

(5) Mohit, A. A.; Martin, J. H.; Miller, C. A. p493F12 kinase: a novel MAP kinase expressed in a subset of neurons in the human nervous system. *Neuron* **1995**, *14*, 67–78.

(6) Holtz, W. A.; Turetzky, J. M.; Jong, Y. J.; O'Malley, K. L. Oxidative stress-triggered unfolded protein response is upstream of intrinsic cell death evoked by parkinsonian mimetics. *J. Neurochem.* **2006**, *99*, 54–69.

(7) Pan, J.; Xiao, Q.; Sheng, C. Y.; Hong, Z.; Yang, H. Q.; Wang, G.; Ding, J. Q.; Chen, S. D. Blockade of the translocation and activation of c-Jun N-terminal kinase 3 (JNK3) attenuates dopaminergic neuronal damage in mouse model of Parkinson's disease. *Neurochem. Int.* **2009**, *54*, 418–25.

(8) Peng, J.; Mao, X. O.; Stevenson, F. F.; Hsu, M.; Andersen, J. K. The herbicide paraquat induces dopaminergic nigral apoptosis through sustained activation of the JNK pathway. *J. Biol. Chem.* **2004**, *279*, 32626–32.

(9) Luo, Y.; Umegaki, H.; Wang, X.; Abe, R.; Roth, G. S. Dopamine induces apoptosis through an oxidation-involved SAPK/JNK activation pathway. *J. Biol. Chem.* **1998**, *273*, 3756–64.

(10) Swahn, B. M.; Huerta, F.; Kallin, E.; Malmstrom, J.; Weigelt, T.; Viklund, J.; Womack, P.; Xue, Y.; Ohberg, L. Design and synthesis of 6-anilinoindazoles as selective inhibitors of c-Jun N-terminal kinase-3. *Bioorg. Med. Chem. Lett.* **2005**, *15*, 5095–5099.

(11) Kamenecka, T.; Habel, J.; Duckett, D.; Chen, W.; Ling, Y. Y.; Frackowiak, B.; Jiang, R.; Shin, Y.; Song, X.; LoGrasso, P. Structure-activity relationships and X-ray structures describing the selectivity of aminopyrazole inhibitors for c-Jun N-terminal kinase 3 (JNK3) over p38. *J. Biol. Chem.* **2009**, *284*, 12853–12861.

(12) Swahn, B. M.; Xue, Y.; Arzel, E.; Kallin, E.; Magnus, A.; Plobeck, N.; Viklund, J. Design and synthesis of 2′-anilino-4,4′-bipyridines as selective inhibitors of c-Jun N-terminal kinase-3. *Bioorg. Med. Chem. Lett.* **2006**, *16*, 1397–1401.

(13) Szczepankiewicz, B. G.; Kosogof, C.; Nelson, L. T.; Liu, G.; Liu, B.; Zhao, H.; Serby, M. D.; Xin, Z.; Liu, M.; Gum, R. J.; Haasch, D. L.; Wang, S.; Clampit, J. E.; Johnson, E. F.; Lubben, T. H.; Stashko, M. A.; Olejniczak, E. T.; Sun, C.; Dorwin, S. A.; Haskins, K.; Abad-Zapatero, C.; Fry, E. H.; Hutchins, C. W.; Sham, H. L.; Rondinone, C. M.; Trevillyan, J. M. Aminopyridine-based c-Jun N-terminal kinase inhibitors with cellular activity and minimal cross-kinase activity. *J. Med. Chem.* **2006**, *49*, 3563–3580.

(14) Zhao, H.; Serby, M. D.; Xin, Z.; Szczepankiewicz, B. G.; Liu, M.; Kosogof, C.; Liu, B.; Nelson, L. T.; Johnson, E. F.; Wang, S.; Pederson, T.; Gum, R. J.; Clampit, J. E.; Haasch, D. L.; Abad-Zapatero, C.; Fry, E. H.; Rondinone, C.; Trevillyan, J. M.; Sham, H. L.; Liu, G. Discovery of potent, highly selective, and orally bioavailable pyridine carboxamide c-Jun NH2-terminal kinase inhibitors. *J. Med. Chem.* **2006**, *49*, 4455–4458.

(15) Angell, R. M.; Atkinson, F. L.; Brown, M. J.; Chuang, T. T.; Christopher, J. A.; Cichy-Knight, M.; Dunn, A. K.; Hightower, K. E.; Malkakorpi, S.; Musgrave, J. R.; Neu, M.; Rowland, P.; Shea, R. L.; Smith, J. L.; Somers, D. O.; Thomas, S. A.; Thompson, G.; Wang, R. *N*-(3-Cyano-4,5,6,7-tetrahydro-1-benzothien-2-yl)-amides as potent, selective, inhibitors of JNK2 and JNK3. *Bioorg. Med. Chem. Lett.* **2007**, *17*, 1296–1301.

(16) Gaillard, P.; Jeanclaude-Etter, I.; Ardissone, V.; Arkinstall, S.; Cambet, Y.; Camps, M.; Chabert, C.; Church, D.; Cirillo, R.; Gretener, D.; Halazy, S.; Nichols, A.; Szyndralewiez, C.; Vitte, P. A.; Gotteland, J. P. Design and synthesis of the first generation of novel potent, selective, and in vivo active (benzothiazol-2-yl)acetonitrile inhibitors of the c-Jun N-terminal kinase. *J. Med. Chem.* **2005**, *48*, 4596–4607.

(17) Jiang, R.; Duckett, D.; Chen, W.; Habel, J.; Ling, Y. Y.; LoGrasso, P.; Kamenecka, T. M. 3,5-Disubstituted quinolines as novel c-Jun N-terminal kinase inhibitors. *Bioorg. Med. Chem. Lett.* **2007**, *17*, 6378–6382.

(18) Alam, M.; Beevers, R. E.; Ceska, T.; Davenport, R. J.; Dickson, K. M.; Fortunato, M.; Gowers, L.; Haughan, A. F.; James, L. A.; Jones, M. W.; Kinsella, N.; Lowe, C.; Meissner, J. W.; Nicolas, A. L.; Perry, B. G.; Phillips, D. J.; Pitt, W. R.; Platt, A.; Ratcliffe, A. J.; Sharpe, A.; Tait, L. J. Synthesis and SAR of aminopyrimidines as novel c-Jun N-terminal kinase (JNK) inhibitors. *Bioorg. Med. Chem. Lett.* **2007**, *17*, 3463–3467.

(19) Humphries, P. S.; Lafontaine, J. A.; Agree, C. S.; Alexander, D.; Chen, P.; Do, Q. Q.; Li, L. Y.; Lunney, E. A.; Rajapakse, R. J.; Siegel, K.; Timofeevski, S. L.; Wang, T.; Wilhite, D. M. Synthesis and SAR of 4-substituted-2-aminopyrimidines as novel c-Jun N-terminal kinase (JNK) inhibitors. *Bioorg. Med. Chem. Lett.* **2009**, *19*, 2099–2102.

(20) LoGrasso, P.; Kamenecka, T. Inhibitors of c-jun-N-terminal kinase (JNK). *Mini Rev. Med. Chem.* **2008**, *8*, 755–766.

(21) Lee, M. R.; Dominguez, C. MAP kinase p38 inhibitors: clinical results and an intimate look at their interactions with p38alpha protein. *Curr. Med. Chem.* **2005**, *12*, 2979–2994.

(22) Carboni, S.; Boschert, U.; Gaillard, P.; Gotteland, J. P.; Gillon, J. Y.; Vitte, P. A. AS601245, a c-Jun NH2-terminal kinase (JNK) inhibitor, reduces axon/dendrite damage and cognitive deficits after global cerebral ischaemia in gerbils. *Br. J. Pharmacol.* **2008**, *153*, 157–163.

(23) Carboni, S.; Hiver, A.; Szyndralewiez, C.; Gaillard, P.; Gotteland, J. P.; Vitte, P. A. AS601245 (1,3-benzothiazol-2-yl (2-[[2-(3-pyridinyl) ethyl] amino]-4 pyrimidinyl) acetonitrile): a c-Jun NH2-terminal protein kinase inhibitor with neuroprotective properties. *J. Pharmacol. Exp. Ther.* **2004**, *310*, 25–32.

(24) Ember, B.; Kamenecka, T.; LoGrasso, P. Kinetic mechanism and inhibitor characterization for c-jun-N-terminal kinase 3alpha1. *Biochemistry* **2008**, *47*, 3076–3084.

(25) Fricker, M.; LoGrasso, P.; Ellis, S.; Wilkie, N.; Hunt, P.; Pollack, S. J. Substituting c-Jun N-terminal kinase-3 (JNK3) ATP-binding site amino acid residues with their p38 counterparts affects binding of JNK- and p38-selective inhibitors. *Arch. Biochem. Biophys.* **2005**, *438*, 195–205.

(26) Scapin, G.; Patel, S. B.; Lisnock, J.; Becker, J. W.; LoGrasso, P. V. The structure of JNK3 in complex with small molecule inhibitors: structural basis for potency and selectivity. *Chem. Biol.* **2003**, *10*, 705–712.

(27) Dominguez, C.; Powers, D. A.; Tamayo, N. p38 MAP kinase inhibitors: many are made, but few are chosen. *Curr. Opin. Drug Discovery Dev.* **2005**, *8*, 421–430.

(28) Wood, E. R.; Truesdale, A. T.; McDonald, O. B.; Yuan, D.; Hassell, A.; Dickerson, S. H.; Ellis, B.; Pennisi, C.; Horne, E.; Lackey, K.; Alligood, K. J.; Rusnak, D. W.; Gilmer, T. M.; Shewchuk, L. A unique structure for epidermal growth factor receptor bound to GW572016 (Lapatinib): relationships among protein conformation, inhibitor off-rate, and receptor activity in tumor cells. *Cancer Res.* **2004**, *64*, 6652–6659.

(29) Kelder, J.; Grootenhuis, P. D.; Bayada, D. M.; Delbressine, L. P.; Ploemen, J. P. Polar molecular surface as a dominating determinant for oral absorption and brain penetration of drugs. *Pharm. Res.* **1999**, *16*, 1514–1519.

(30) Martin, Y. C. A bioavailability score. *J. Med. Chem.* **2005**, *48*, 3164–3170.

(31) Ventura, J. J.; Cogswell, P.; Flavell, R. A.; Baldwin, A. S., Jr.; Davis, R. J. JNK potentiates TNF-stimulated necrosis by increasing the production of cytotoxic reactive oxygen species. *Genes Dev.* **2004**, *18*, 2905–2915.

(32) Kamata, H.; Honda, S.; Maeda, S.; Chang, L.; Hirata, H.; Karin, M. Reactive oxygen species promote TNFalpha-induced death and sustained JNK activation by inhibiting MAP kinase phosphatases. *Cell* **2005**, *120*, 649–661.

(33) Curtin, J. F.; Donovan, M.; Cotter, T. G. Regulation and measurement of oxidative stress in apoptosis. *J. Immunol. Methods* **2002**, *265*, 49–72.
(34) Fan, M.; Goodwin, M.; Vu, T.; Brantley-Finley, C.; Gaarde, W. A.; Chambers, T. C. Vinblastine-induced phosphorylation of Bcl-2 and Bcl-XL is mediated by JNK and occurs in parallel with inactivation of the Raf-1/MEK/ERK cascade. *J. Biol. Chem.* **2000**, *275*, 29980–29985.
(35) Kharbanda, S.; Saxena, S.; Yoshida, K.; Pandey, P.; Kaneki, M.; Wang, Q.; Cheng, K.; Chen, Y. N.; Campbell, A.; Sudha, T.; Yuan, Z. M.; Narula, J.; Weichselbaum, R.; Nalin, C.; Kufe, D. Translocation of SAPK/JNK to mitochondria and interaction with Bcl-x(L) in response to DNA damage. *J. Biol. Chem.* **2000**, *275*, 322–327.
(36) Papadakis, E. S.; Finegan, K. G.; Wang, X.; Robinson, A. C.; Guo, C.; Kayahara, M.; Tournier, C. The regulation of Bax by c-Jun N-terminal protein kinase (JNK) is a prerequisite to the mitochondrial-induced apoptotic pathway. *FEBS Lett.* **2006**, *580*, 1320–1326.
(37) Sunayama, J.; Tsuruta, F.; Masuyama, N.; Gotoh, Y. JNK antagonizes Akt-mediated survival signals by phosphorylating 14−3-3. *J. Cell Biol.* **2005**, *170*, 295–304.
(38) Abdelli, S.; Puyal, J.; Bielmann, C.; Buchillier, V.; Abderrahmani, A.; Clarke, P. G.; Beckmann, J. S.; Bonny, C. JNK3 is abundant in insulin-secreting cells and protects against cytokine-induced apoptosis. *Diabetologia* **2009**, *52*, 1871–1880.
(39) Cohen, A. E.; Ellis, P. J.; Miller, M. D.; Deacon, A. M.; Phizackerley, R. P. *J.* An automated system to mount cryo-cooled protein crystals on a synchrotron beamline, using compact sample cassettes and a small-scale robot. *J. Appl. Crystallogr.* **2002**, *35*, 720–726.
(40) Otwinowski, Z.; Minor, W. Processing of X-ray diffraction data collected in oscillation mode. *Methods Enzymol.* **1997**, *276*, 307–326.
(41) McCoy, A. J.; Grosse-Kunstleve, R. W.; Adams, P. D.; Winn, M. D.; Storoni, L. C.; Read, R. J. Phaser crystallographic software. *J. Appl. Crystallogr.* **2007**, *40*, 658–674.
(42) Murshudov, G. N.; Vagin, A. A.; Dodson, E. J. Application of Maximum Likelihood Refinement. *Acta Crystallogr., Sect. D: Biol. Crystallogr.* **1997**, *53*, 240–255.
(43) Emsley, P.; Cowtan, K. Coot: model-building tools for molecular graphics. *Acta Crystallogr., Sect. D: Biol. Crystallogr.* **2004**, *60*, 2126–2132.
(44) PROJECT, C. C. The CCP4 Suite: Programs for Protein Crystallography. *Acta Crystallogr., Sect. D: Biol. Crystallogr.* **1994**, *50*, 760−763.
(45) Lovell, S. C.; Davis, I. W.; Arendall, W. B., III; de Bakker, P. I. W.; Word, J. M.; Prisant, M. G.; Richardson, J. S.; Richardson, D. C. Structure validation by C-alpha geometry: phi, psi, and C-beta deviation. *Proteins: Structure, Function, and Genetics* **2003**, *50*, 437–450.
(46) DeLano, W. L. *The PyMol Molecular Graphics System*; DeLano Scientific: San Carlos, CA, 2002.